

Numerical Modeling of the Three-Dimensional Magnetic Fields and Eruption in the Solar Active Region 11158

INOUE, Satoshi^{1*}

¹School of Space Research, Kyung Hee University

Solar flares and coronal mass ejections (CMEs) are considered as sudden liberation of magnetic energy in the solar corona, which affect geospace in the form of electromagnetic disturbance called geomagnetic storms. Unfortunately, measurement based on vector field observations only provide the two-dimensional information of magnetic field on the photosphere, therefore, we could not reach on a common understanding yet regarding to the three-dimensional (3D) magnetic structure causing the eruptive phenomena and associated dynamics. In order to clarify them, in this study we first extrapolate a 3D coronal magnetic field under the Nonlinear Force-Free Field (NLFFF) approximation based on the vector field, using the Magnetohydrodynamic (MHD) relaxation method developed by Inoue et al. 2014, and then compare the 3D structures before and after the flare. Next we perform an MHD simulation to clarify the dynamics during the flare where the NLFFF prior to the flare is set as an initial condition. Photospheric vector field was observed at 00:00 UT and 03:00 UT on February 15 corresponding to before and after the X2.2-class flare taking place around at 01:50 UT, taken by the Helioseismic And Magnetic Imager (HMI) on board the Solar Dynamics Observatory (SDO) satellite.

As a result, we found that the NLFFF has strongly twisted field lines; most of them are in the range from half-turn to one turn twist, being resided above the polarity inversion line. Furthermore, we found that a distribution of these footpoints well captures the flare ribbons observed by Hinode where Ca II emission is strongly enhanced. On the other hand, because the most of these strongly twisted lines disappear after the flare, consequently the twisted field lines having more than half-turn twist play an important role on causing the large flare. The MHD simulation successfully shows an eruption of the more strongly twisted lines whose values are over one-turn twist, which are produced through the magnetic reconnection in strongly twisted lines of the NLFFF. Eventually, we found that they exceed a critical height at which the flux tube becomes unstable to the torus instability determining the condition that whether a flux tube might escape from the overlying field lines or not. In addition to these, during the eruption, we found that the distribution of the observed two-ribbon flares is similar to the spatial variance of the footpoints caused by the reconnection of strongly twisted lines with more than half-turn twist. Furthermore, because the post flare loops obtained from MHD simulation well capture that in EUV image taken by SDO, these results support the reliability of our simulation.

Keywords: Active Region, Coronal Magnetic Field, Solar Flare, Coronal Mass Ejections, Numerical Modeling

Study on Triggering Process of Solar Flare on the basis of Satellite Observation

BAMBA, Yumi^{1*} ; KUSANO, Kanya¹ ; IMADA, Shinsuke¹

¹STEL, Nagoya Univ.

Solar Flares are explosive phenomena driven by magnetic energy stored in the solar corona. Because interplanetary disturbances associated with solar flares sometimes impact terrestrial environments and infrastructure, understanding the flare-triggering process is important not only from a solar physics perspective but also for space weather forecasting. There are numerous observational studies and simulations which attempted to reveal the onset mechanism of solar flares. Because different observations support different models, the underlying mechanism of flare onset remains elusive. Thus the predictability of flare occurrence remains limited.

We have analyzed several flare events obtained by the Solar Optical Telescope (SOT) onboard the Hinode Satellite in order to elucidate flare trigger mechanism [Bamba *et al.* 2013]. We investigated the spatio-temporal correlation between the detailed magnetic field structure and the chromospheric pre-flare emission at the central part of flaring regions for several hours prior to the onset of flares. We observed that the magnetic shear angle in the flaring regions exceeded 70 degrees, as well as that characteristic magnetic disturbances developed at the centers of flaring regions in the pre-flare phase. The observed signatures strongly support the idea of flare trigger mechanism presented by Kusano *et al.* (2012), which proposed that solar flares can be triggered by the interaction between the sheared arcade and one of the two types of small magnetic disturbances. Hence, we could classify the events into two groups depending on the structure of their magnetic polarity inversion lines; to the so-called "Opposite-Polarity (OP)" and "Reversed-Shear (RS)" magnetic field. Furthermore, we studied how small magnetic field can work for triggering flares based on the Hinode observations. The results indicate that the critical amount of magnetic flux for the small magnetic field to trigger flares, depends on the magnetic connectivity in the flaring site, and it varies even within an active region.

However, only four Hinode data sets have been utilizable for the analyze of this study because of the SOT's limited field of view (FOV) (328" × 164" for Narrow-band Filter Imager, 218" × 109" for Broad-band Filter Imager). Therefore, we applied the analysis method of Bamba *et al.* (2013) to the data obtained by the Helioseismic and Magnetic Imager (HMI) and the Atmospheric Imaging Assembly (AIA) onboard the Solar Dynamics Observatory (SDO), which has a full-disk FOV (2000" × 2000") in order to increase the number of event analysis. We chose the flare events observed by SDO until 31 Jan. 2014, larger than M5.0 GOES class. Eleven X-class and twenty M-class events meet this condition, and we classified these events into independent 6 types by using following three conditions: (1) whether the initial flare kernels has obvious and sheared two-ribbon structure, (2) whether the chromospheric brightening was observed at the center of sheared ribbon, (3) the results of measurement of the magnetic shear angle θ and the azimuth of flare trigger field ϕ .

In this presentation, we would like to report the result of comparative study of Hinode and SDO. We would like to also introduce our preliminary result of statistical flare trigger study using SDO/HMI and AIA.

References:

- [1] *Study on Triggering Process of Solar Flares Based on Hinode/SOT Observations*,
Y. Bamba, K. Kusano, T. T. Yamamoto, and T. J. Okamoto,
2013 *ApJ* 778 48 doi:10.1088/0004-637X/778/1/48
- [2] *Magnetic Field Structures Triggering Solar Flares and Coronal Mass Ejections*,
K. Kusano, Y. Bamba, T. T. Yamamoto, Y. Iida, S. Toriumi, and A. Asai,
2012 *ApJ* 760 31 doi:10.1088/0004-637X/760/1/31

Keywords: Sun, solar flare, magnetic field, SDO, Hinode, space weather

X5.4 flare on 7 March 2012: magnetic and velocity properties at the solar surface

SHIMIZU, Toshifumi^{1*} ; LITES, Bruce² ; BAMBA, Yumi³

¹ISAS/JAXA, ²HAO/NCAR, ³Nagoya University

Solar flares abruptly release the free energy stored as a non-potential magnetic field in the corona and may be accompanied by eruptions of the coronal plasma. Formation of non-potential magnetic field and the mechanisms on triggering the onset of flares are still unclear; Especially, dynamical behaviors observed around polarity inversion lines producing major flares observationally. This presentation will discuss X5.4 flare on 7 March 2012 with emphasis on magnetic and velocity field properties at the solar surface. The coronal mass ejection launched at the same time as the X5.4 flare propagated through interplanetary space and caused a large geomagnetic storm on 9 March. One of remarkable properties to be discussed is a high-speed material flow existing along the polarity inversion line located between flare ribbons at the main energy release side. The high-speed material flow was observed in the horizontally oriented magnetic field formed nearly in parallel to the polarity inversion line and it existed at least from 6 hours before the onset of the flare and continued at least for several hours after the onset of the flare. Observations suggest that the observed material flow represents neither the emergence nor convergence of the magnetic flux. It may be rather considered as material flows working for increasing the magnetic shear along the polarity inversion line and for developing the magnetic structures favorable for the onset of the eruptive flare.

Keywords: solar flare, Hinode, X-ray, Optical, magnetic field, Doppler shift

Estimation of Astronaut Dose inside the Kibo Module during Large Solar Flare Events

SATO, Tatsuhiko^{1*} ; KATAOKA, Ryuhō² ; NAGAMATSU, Aiko³

¹Japan Atomic Energy Agency, ²National Institute of Polar Research, ³Japan Aerospace Exploration Agency

Forecast of radiation doses for astronauts as well as aircrews due to the exposure to solar energetic particles (SEP) is one of the greatest challenges in space weather research. In last 3 years, we have developed a warning system of aviation exposure to solar energetic particles: WASAVIES, which can predict the SEP doses at any flight conditions within 2.5 hours after the onset of ground level enhancements (GLE). In this system, the SEP fluxes incident to the atmosphere are calculated by physics-based models [1,2], and they are converted to radiation doses using a database developed on the basis of air-shower simulation [3]. In this study, we applied the same physics-based models to the estimate of the SEP fluxes on the orbit of International Space Station, and converted the fluxes to radiation doses for astronauts staying inside the Kibo module. For this conversion, we performed Monte Carlo cosmic-ray transport simulation, using the Particle and Heavy Ion Transport code System PHITS [4] in combination with the realistic 3D model of the Kibo module. A brief outline of WASAVIES together with the results of the astronaut dose estimation will be presented at the meeting.

[1] Y. Kubo, submitted to Space Weather

[2] R. Kataoka et al. submitted to Space Weather

[3] T. Sato et al. (2013) Radiat. Prot. Dosim. doi:10.1093/rpd/nct332

[4] T. Sato et al. (2013) J. Nucl. Sci. Technol. 50, 913-923. <http://phits.jaea.go.jp/>

Keywords: solar flare, radiation dose, solar energetic particle, astronaut, space weather, PHITS

WASAVIES: Warning System for Aviation Exposure to Solar Energetic Particles

KATAOKA, Ryuho^{1*} ; SATO, Tatsuhiko² ; KUBO, Yuki³ ; SHIOTA, Daikou⁴ ; KUWABARA, Takao⁵ ; YASHIRO, Seiji⁶ ; YASUDA, Hiroshi⁷

¹NIPR, ²JAEA, ³NICT, ⁴Nagoya University, ⁵Delaware University, ⁶CUA, ⁷NIRS

Solar energetic particles (SEP) sometimes induce air shower that significantly increase the radiation dose at flight altitudes. In order to inform the situation of such a space radiation hazard to aircrews, a physics-based forward model is developed as WASAVIES (Warning System for Aviation Exposure to SEP) based on focused transport equation and Monte Carlo particle transport simulation code PHITS. WASAVIES gives the fastest and simplest way to predict the time profile of dose rate during ground-level enhancements (GLEs).

Keywords: solar proton, radiation dose, flares, air shower

Plan of large SPE search by the ^{14}C content measurement in Japanese trees for the past 5000 years

MIYAKE, Fusa^{1*} ; MASUDA, Kimiaki¹ ; HAKOZAKI, Masataka² ; NAKAMURA, Toshio² ; KIMURA, Katsuhiko³

¹Solar-Terrestrial Environment Laboratory, Nagoya University, ²Center for Chronological Research, Nagoya University, ³Faculty of Symbiotic Systems Science, Fukushima University

Radiocarbon (^{14}C) is produced by incoming cosmic rays to the Earth. Produced ^{14}C becomes $^{14}\text{CO}_2$ and is absorbed by trees by photosynthesis. Then, tree-rings record the past cosmic ray intensity. Rapid yearly increases in the ^{14}C content have been detected for the period from AD 774 to AD 775 and from AD 993 to AD 994. Although some candidates for the cause of these cosmic-ray events have been considered, it has been considered that the solar activity (large SPE) is the most plausible cause.

There is the possibility that a lot of ^{14}C increase events like the AD 775 one are hidden in the periods when the ^{14}C content has not been measured with a 1-year resolution. If we detect such events, we are able to discuss a detailed occurrence rate of large SPE which is very important factor to prepare for future large SPEs.

We are planning to search for ^{14}C increase events by the measurements of ^{14}C content in Japanese trees for this 5000 years. In this thesis, we are going to explain the plan and problems.

Keywords: radiocarbon, tree-rings, cosmic-ray, SPE

End-Cretaceous mass extinction driven by the encounter with a dark cloud

NIMURA, Tokuhiko^{1*}; EBISUZAKI, Toshikazu²; MARUYAMA, Shigenori³

¹Okayama Astronomical Museum, ²RIKEN, ³Earth-Life Science Institute, Tokyo Institute of Technology

We found that a significant positive broad component of iridium in a pelagic deep sea sediment core (886C) around an iridium peak by asteroid impact corresponds at the K-Pg boundary. The 886C is core sample was taken by the Ocean Drilling Program (ODP) in the central portion of the North Pacific. This site has been in Pelagic from the End-Cretaceous periods. The accumulation rate is 0.5 m Myr⁻¹. Kyte et al., (1995) measured iridium density in the 886C core of 0.75-72.2 m which corresponds of ~80 Ma from the present. In this data, there is one sharp peak around 65.5 m correspond at K-Pg boundary. In addition, we found that there are broad components across ~20 m above the background which have some sharp peak component. The Ir value of the broad component which is about dozen times of background. This broad component is difficult to be explained by the materials on the surface of the Earth, and requires the contribution from the iridium-rich extraterrestrial materials, such as CI chondrite. And it is difficult to explain the broad component by diffusion and bioturbation of an iridium peak by asteroid impact. Platinum-group-element such as Pt, Re and Ir are redistributed by changes in sedimentary redox condition. However such change can probably account for many of small <10 cm (Colodner et al., 1992) and the mean global depth of marine bioturbation was calculated to be 9.8±4.5 cm (Boudreau, 1994). And also an evidence of bioturbation was not found from lithofacies (Proc. ODP, Init. Repts., 145).

We consider that the broad component can be caused by an encounter of the solar system with a dark cloud with a size of ~100 pc and the central density of over 2000 protons/cc in the galactic disk and estimated that the flux of exosolar material began ~73 Ma and has run through ~8 Myr. By the Kataoka's "Nebula Winter model" (Kataoka 2013), dark cloud can lead to an environmental catastrophe to the Earth from a few kiloyear to megayear. The dark cloud encounter enhances a flux of cosmic dust particles and cosmic rays which lead to global cooling and destruction of the ozone layer.

The solid particles from the dark cloud accrete on the Earth and in the stratosphere, stay for a several months; their sunshield effect is as large as -9.3 W m⁻². The climate cooling in the End-Cretaceous period is also suggested by the variations of stable isotope ratios in oxygen and strontium (Brian and Huber, 1990; Barrera and Savin, 1999; Li and Keller, 1998). Any photosynthetic plants had heavily damaged, and loss of biodiversity began to the top of food chain.

The mass extinction at K-Pg boundary, which is widely thought to be caused by an impact of an asteroid (e. g., Schulte et al., 2010). However, a complete extinction of level of family by asteroid impact seems rather difficult. First, a severe environment turn-over would finish few years after impact, the solid particles and sulphate launched by the asteroid impact was settled down for only few month (troposphere) to few years (stratosphere) and negative radiative forcing became negligible after a few years from the impact (Pierazzo, 2001). The number of individuals would recover completely after the environmental catastrophe was over, if a few percent of individuals of one species survived.

Second, in spite of there were similar impacts without catastrophic on the Earth, for example, Alamo, Woodleigh, and Popigai crater, there are no evidences of association for extinction. However, because the encounter with the dark cloud perturbs the orbit of asteroid or comet by its gravitational potential and may lead an asteroid or comet shower, the asteroid impact at K-Pg may be one of the consequences of the dark cloud. For a certainly, only an asteroid impact cannot involve mass extinction, however may be role cruncher. The multiple impact and volcanism in a short period of time (Keller, 2005) may have been caused by encounter the dark nebula and attendant cosmic ray, respectively.

Keywords: Nebula Winter, dark cloud, mass extinction, End-Cretaceous, K-Pg boundary, Ocean Drilling Program

Update on the US GIC activities and generation of benchmark geomagnetic disturbance (GMD) scenarios

PULKKINEN, Antti^{1*}

¹NASA GSFC

The awareness about potential major impacts of geomagnetically induced currents (GIC) has drawn a high level action in the US and in Canada. More specifically, regulatory process has been launched to generate standards for GIC hazard assessments and mitigation procedures. All US high-voltage power transmission-related entities need to follow the standards in the near future. One of the central GIC activities in the US has been the North the American Electric Reliability Corporation's (NERC) GMD Task Force that has allowed in-depth communication and collaboration between US federal organizations, power transmission operators and scientific research community. I will discuss these activities in this paper and outline the road ahead for some of the key US GIC activities.

As a part of the GMD standards drafting process and the US GIC hazards assessments, substantial effort has been made for generating benchmark GMD scenarios. These scenarios that quantify extreme geoelectric field magnitudes and temporal waveforms of the field fluctuations are the foundation for subsequent engineering analyses. The engineering analyses will include the transmission system voltage stability and transformer heating assessments. The work on the GMD scenarios has been a major collaboration between a number of US and Canadian entities involved in GMD research and transmission system operations. I will discuss in this paper also the key elements of the benchmark GMD generation process and show the latest results from our NASA GSFC work on the topic.

Keywords: Space weather, geomagnetically induced currents, Extreme events

Spatial distribution of nonthermal electrons in an X-class flare on 13 May 2013

MASUDA, Satoshi^{1*}

¹STEL, Nagoya Univeristy

Four X-class flares took place in May 2013. Fortunately three of four were observed with Nobeyama Radioheliograph (NoRH). One of them occurred behind the east limb on 13 May 2013. It is a good chance to investigate the height distribution of nonthermal electrons in the solar corona. In the framework of the standard flare model based on magnetic reconnection, Minoshima et al. (2011) showed that the height distribution of accelerated/heated electrons depends on the energy of the electrons. NoRH has a capability to observe a solar flare in 17 and 34 GHz with a high time resolution (100 ms). The energy of electrons emitting microwaves is very high (~MeV), and the mean-energy emitting 34 GHz is higher than that for 17 GHz. Hard X-rays are emitted by relatively lower-energy (~100 keV) electrons. So this dataset can cover a wide energy range of accelerated electrons. In order to understand the electron acceleration/transport/loss processes, multi-wavelength observation is crucially important. The 13 May 2013 flare was simultaneously observed with NoRH and RHESSI (The Reuven Ramaty High Energy Solar Spectroscopic Imager). Investigating the distribution of these emission sources in the solar corona, we discuss the electron acceleration/transport/loss processes.

Keywords: solar flare, particle acceleration, microwave, hard X-ray, solar corona, magnetic reconnection

An energetics study of X-ray jets using Hinode/XRT observation

SAKO, Nobuharu^{1*} ; SHIMOJO, Masumi² ; WATANABE, Tetsuya² ; SEKII, Takashi²

¹The Graduate University for Advanced Studies, ²National Astronomical Observatory of Japan

For plasma acceleration in X-ray jets in the solar corona, three mechanisms have been considered, based on the model of X-ray jets by magnetic reconnection (Shibata et al. 1992); The reconnection jet produced by magnetic tension, the evaporation flow produced by pressure gradient, and the twisted jet produced by magnetic pressure. There are some evidences of X-ray jets in active regions (ARs) produced by pressure gradient. On the other hands, there is no observational evidence of X-ray jets by the other forces except the result of a high-speed jet. In order to distinguish the evaporation flow from the other types of jets, I have studied the energetics of the X-ray jets.

Using over 100 X-ray jets greater than 3×10^4 km in length in ARs, quiet regions (QRs), and coronal holes (CHs), I have found no large differences in the life time, the width of the jets, and the area of the footpoint flares in such regions. On the other hands, the plasma number density of the X-ray jets and flares in ARs is ten times larger than those in QRs and CHs. Assuming the energy balance between conductive flux and heat flux by the footpoint flare, we estimate the temperature of the jets. The AR jets has a wide range of the temperature (1 MK-9 MK), while the temperature of most X-ray jets in CH and QR is 1~2 MK. In my presentation, I will discuss a relationship of the speed with the temperature of the jets.

Keywords: Sun, Solar Corona, X-ray jet, Energy release, Hinode

Lower temperature response of an EUV wave observed by Hinode/EIS and SDO/AIA

LEE, Kyoung sun^{1*} ; KWON, Ryun young² ; BROOKS, David² ; SHIMIZU, Toshifumi¹

¹ISAS/JAXA, ²George Mason University

We investigate an EUV wave observed by Hinode/EIS and SDO/AIA on 2011 August 04. The EUV wave propagates across the solar disk and the wave front passing through a remote active region (AR 11263) is observed by EIS. This EUV wave has already been analyzed using coronal lines, but the lower temperature response to the EUV wave has not been investigated. Using multi-wavelength observations from EIS and AIA, we determined the intensity and Doppler velocity variation of different temperature lines and compared them. From the comparison, we found an enhancement of the intensity at lower temperatures before the intensity increase seen in the coronal filters of AIA. And a significant enhancement of the red shift (10 km/s) in the lower temperature line (Si VII, $\log T \sim 5.8$) compared to the increase of the red shift (~ 3 km/s) in coronal lines (Fe XII, FeXIII, and Si X, $\log T \sim 6.1-6.2$) when the EUV wave interacts with the active region. We will discuss the impact of the EUV wave on the lower temperature emission.

Keywords: Spectroscopy, Corona, EUV wave

Imaging, spectroscopic and stereoscopic observations of the bi-directional inflow in the solar flare

MATSUI, Yuki^{1*} ; YOKOYAMA, Takaaki¹

¹University of Tokyo

The standard model of solar flares based on the magnetic reconnection includes bi-directional inflow toward the reconnection point. Corresponding to the bi-directional inflow, high temperature loops like a cusp shape are formed due to the magnetic reconnection. By combination of imaging, spectroscopic and stereoscopic observations, we succeeded in capture the three-dimensional structure of a bi-directional reconnection inflow of a solar flare.

We analyzed a C-class flare that occurred on 2012 September 11 beyond the solar limb. The bi-directional inflow was found in the images of coronal temperature filter taken by AIA onboard SDO. Hinode EUV Imaging Spectrometer (EIS) also observed this flare and provide the Doppler velocity of the bi-directional inflows. At the same time, cusp loops were observed with the raster scans of FeXXIV emission line (over 10 MK) at the region surrounded by the bi-directional inflow. This is clear evidence that 1MK loops are heated over 10MK by the magnetic reconnection. STEREO A/SECCHI was observing this flow from a different line of site. Inflowing angle in STEREO A/SECCHI images is consistent with the angle speculated by apparent velocity of SDO/AIA and line of sight velocity of Hinode/EIS. By combining these data sets, we constructed a self-consistent three-dimensional picture of the flows.

Keywords: solar flare, reconnection

Diagnosis of coronal shock strength using the activation of large amplitude prominence oscillation

TAKAHASHI, Takuya^{1*} ; ASAI, Ayumi² ; SHIBATA, Kazunari³

¹Graduate School of Science, Kyoto University, ²Unit of Synergetic Studies for Space, Kyoto University, ³Kwasan and Hida Observatories, Kyoto University

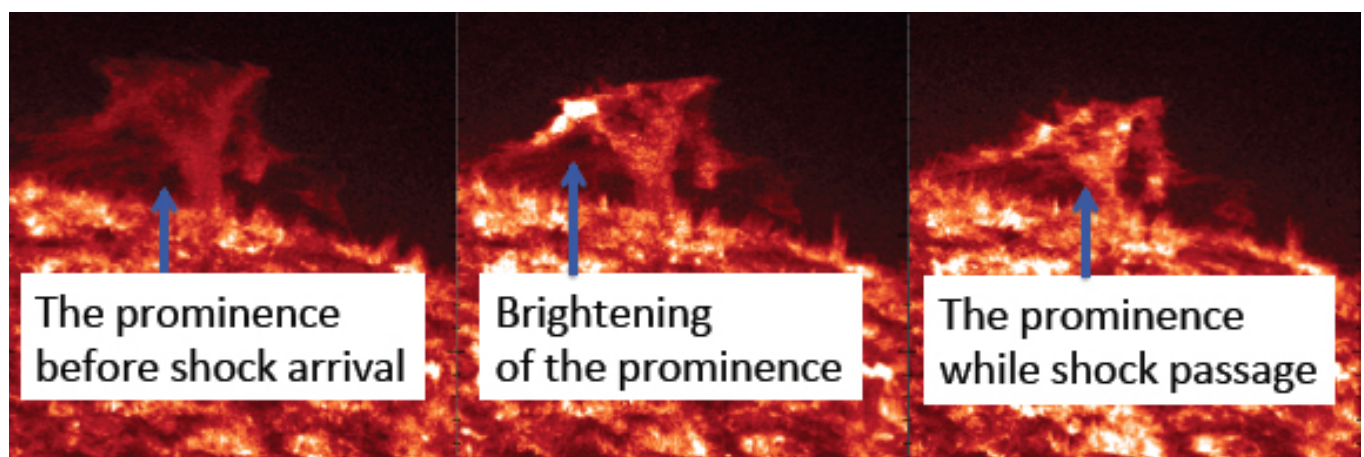
X5.4 class solar flare occurred on March 7, 2012 which was the second largest flare in this solar cycle. The flare was associated with very fast coronal mass ejection (CME) with the velocity of over 2500 km/s. Associated with this flare, a wave-like coronal disturbance (known as EUV wave) was observed to propagate along the solar surface. The observed EUV wave propagated with the average speed of about 670 km/s towards the north and 'hit' a polar prominence leading to its large amplitude oscillation. The activated prominence strongly brightened when EUV wave 'pushed' it.

Because of the difficulty in direct observation of physical quantities in the corona, the physical nature of the EUV waves is still under discussion. Two main interpretations of EUV waves are the 'fast mode MHD wave/shock' interpretation, and 'non-wave' interpretations.

In the images taken with Inner coronagraph (COR1) of the Sun Earth Connection Corona and Heliospheric Investigation (SECCHI) on board *Solar Terrestrial Relations Observatory (STEREO)-Behind*, we could see a coronal disturbance detached from expanding CME plasma. The time evolution of the disturbance seen in COR1 images was consistent with that of observed EUV wave. Also, Type II radio burst which is thought to be evidence of coronal shock wave was observed simultaneously. Because of that observational evidence, we regard the observed EUV wave as MHD fast mode shock front. Assuming the shock nature of the observed EUV wave, we could also explain prominence acceleration and brightening consistently.

Using the initial velocity of activated prominence, we could estimate the coronal shock strength of the EUV wave with the help of linear wave theory. We also check the applicability of linear theory to the shock problem with one dimensional numerical model and ascertained that it is applicable when the shock strength is not strong. Estimated fast mode mach number of the EUV wave was between 1.20 and 1.42, and we could say that the EUV wave was a weak shock front in the corona.

Keywords: solar flare, coronal mass ejection (CME), shock waves, solar prominence, magnetohydrodynamics (MHD)



Influence of interplanetary solar wind sector polarity on the ionosphere

LIU, Jing^{1*}

¹Beijing National Observatory of Space Environment, Institute of Geology and Geophysics, CAS

Knowledge of solar sector polarity effects on the ionosphere may provide some clues in understanding of the ionospheric day-to-day variability and 'hysteresis' effect on foF2. In this study, a solar-terrestrial connection ranging from solar sector boundary crossings, geomagnetic disturbances and ionospheric perturbations has been demonstrated. The increases in interplanetary solar wind speed within three days are seen after SB crossings, while the decreases in solar wind dynamic pressure and magnetic field intensity immediately after SB crossings are confirmed by the superposed epoch analysis results. Furthermore, the interplanetary magnetic field (IMF) Bz component turns from northward to southward in March equinox and June solstice as the Earth passes from a solar sector of outward to inward directed magnetic fields, whereas the reverse situation occurs for the transition from toward to away sectors. The IMF Bz component for the same solar sector polarity has opposite signs between March equinox and September equinox, and also between June solstice and December solstice. In order to know how the ionosphere reacts to the interplanetary solar wind variations linkage of SB crossings, the F2 region critical frequency (foF2) covering about four solar cycles and total electron content (TEC) during 1998-2011 are utilized to extract the related information, revealing that they are not modified significantly and vary within the range of 15% on average. The responses of the ionospheric TEC to SB crossings exhibit complex temporal and spatial variations and have strong dependencies on season, latitude, and solar cycle. This effect is more appreciable in equinoctial months than in solstitial months, which is mainly caused by larger southward Bz components in equinox. In September equinox, latitudinal profile of relative variations of foF2 at noon is featured by depressions at high latitudes and enhancements in low-equatorial latitudes during IMF away sectors. The negative phase of foF2 is delayed at solar minimum relative to it during other parts of solar cycle, which might be associated with the difference in longevity of major interplanetary solar wind drivers perturbing the near-Earth environment in different phases of solar cycle.

Ensemble Data Assimilation for Thermospheric Mass Density Specification and Forecasting

MATSUO, Tomoko^{1*} ; LEE, Ite³ ; ANDERSON, Jeffrey⁴

¹University of Colorado at Boulder, CO, USA, ²National Oceanic and Atmospheric Administration, CO, USA, ³National Central University, Taiwan, ⁴National Center for Atmospheric Research, CO, USA

Even though the Earth's upper atmosphere density is tenuous, it is substantial enough to exert significant drag on orbiting spacecraft and debris. The largest uncertainty in low-Earth orbit prediction is aerodynamic drag estimation. Thermospheric mass density variation is the major source of drag estimation errors at altitudes below about 700 km. This paper demonstrates how the limit of predictability of thermospheric mass density variability can be extended by means of ensemble data assimilation.

To assimilate observations of the thermosphere and ionosphere, we use an ensemble data assimilation procedure constructed with the Data Assimilation Research Testbed and the Thermosphere-Ionosphere Electrodynamics General Circulation Model, two sets of community software offered by NCAR. An important attribute of our approach is that the ionosphere-thermosphere coupling is self-consistently treated in both the forecast model and the assimilation scheme. This enables the inference of unobserved thermospheric states from the relatively plentiful observations of the ionosphere. Given the ever-expanding global navigation satellite infrastructure, this is indeed a promising prospect for upper atmosphere data assimilation. Another relevant strategy is using data assimilation to estimate the model forcing parameters that control states of the thermosphere and ionosphere. In comparison to the lower atmosphere, the upper atmosphere is a dissipative, strongly forced dynamical system, so estimation of model forcing parameters can have a dramatic impact on the quality of ensemble forecasting and assimilation of the upper atmosphere.

In this paper, we present results from our ensemble assimilation experiments with thermospheric mass densities obtained from the accelerometer on board the CHAMP satellite, and electron density profiles obtained from the COSMIC/FORMOSAT-3 mission.

Keywords: thermosphere-ionosphere coupling, data assimilation, parameter and state estimation, thermospheric mass density, aerodynamic drag estimation, LEO orbit prediction

Forecast of ionospheric disturbances using a high-resolution atmosphere-ionosphere coupled model

SHINAGAWA, Hiroyuki^{1*} ; JIN, Hidekatsu¹ ; MIYOSHI, Yasunobu² ; FUJIWARA, Hitoshi³ ; YOKOYAMA, Tatsuhiro¹

¹NICT, ²Kyushu University, ³Seikei University

Space weather forecasts are about to enter a stage incorporating numerical forecasts based on realistic numerical simulation, in addition to conventional methods used by forecasters to make predictions based on observational data and experience. At the National Institute of Information and Communications Technology (NICT) of Japan, we have developed an atmosphere-ionosphere coupled model, which includes the whole neutral atmosphere and the ionosphere. The model is called GAIA (Ground-to-topside model of Atmosphere and Ionosphere for Aeronomy). The present version has spatial resolution of about 1 degree in horizontal direction. In addition, we are also developing a high-resolution regional ionospheric model, which has a horizontal resolution of about 10 km. We plan to combine GAIA and the regional model to reproduce mesoscale ionospheric phenomena, such as plasma bubbles and SED (storm enhanced density). The model will be a useful tool for space weather forecast. We will report previous results, and a plan for the new model.

Keywords: space weather, ionosphere, atmosphere, simulation, model, disturbance

Projection of substorm processes from the plasma sheet to the polar ionosphere

TANAKA, Takashi^{1*}

¹Emeritus Professor, Kyushu University

It has been believed that auroras observed in the ionosphere have their corresponding counterpart in the plasma sheet (Haerendel, 2011). Localized auroral breakup should reveal the location of explosive dissipation in the plasma sheet. Similar correspondence is supposed even during the growth phase. While it is well known that the prebreakup arc breakups first during the substorm, the equatorial location and relating formation mechanism of equatorward arc are long-standing questions in the understanding of the growth phase (Sergeev et al., 2012). Another aurora during the growth phase is the poleward bright arc that is believed to be an ionospheric projection of the reconnection separatrix. Also the equatorward extension of the N-S auroral arc has been suggested to be associated with earthward fast bursty flows (Nishimura et al., 2010). The region of aurora indicates that the width of oval is 7° (64° to 71°), near midnight just prior to the breakup. Pitch angle isotropy boundary at 65.5° is critical for the prebreakup arc, since the isotropy boundary coincides with the prebreakup arc. Seen from the structure of isotropy boundary, the breakup arc is somewhere in the transition region between the dipole-like region and the current sheet region. A phenomenon closely related to the projection of the aurora is the distribution of FAC and its tracing. A traditional understanding for the driver of disturbances is the fast flow, both for the growth phase and the onset. The BBF was expected for a wide range of activity including localized auroral brightenings, N-S auroras and streamers (Nakamura et al., 2001). At the same time, the BBF can be a source of the FAC. The cross-tail current is diverted via downward FAC into the ionosphere on the eastward side of the bubble and is connected to upward FACs west of the bubble. The overall region 1-sense FACs is expected to emerge from 64° to 70° (Yang et al., 2012). The plasma ahead of the bubble is compressed, resulting in a high plasma pressure and the region 2-sense FACs that are as thin as 1° , centered at 63° .

Recent M-I coupling simulation reproduces almost all signatures of the substorm, including the preonset arc, and the onset that start from the low-latitude side of the oval (Tanaka et al., 2010). From the numerical solution just prior to the onset, the BBF region from $x=-10$ Re to $x=-20$ Re in the plasma sheet is projected down along the magnetic field to a quite narrow region in the ionosphere from 65.7° to 66.8° latitudes. Even the outmost field line of the plasma sheet is traced down to 68° latitude in the ionosphere. So that the observed high-latitude part of the oval ($68^\circ\sim 71^\circ$) is outside the plasma sheet. The N-S arc that usually starts from higher latitude than 70° cannot be the reflection of the BBF. Near the midnight, in the numerical solution, the region 1 FAC distributes from 65° to 69° (with strong part $67^\circ\sim 68^\circ$) and the region 2 FAC distributes from 62° to 64° latitude. From this result, the growth phase region 1 FAC cannot be from the plasma sheet. The result of current line tracing shows that the growth phase region 1 FAC extends into the magnetosphere as far as $x=-20$ Re through the east-west flow shear between the tail plasma sheet and the lobe. If we look at only the latitude it is barely possible that the onset FAC starting from the lowest-latitude area of the region 1 FAC around 65° could be from the CW that should be inside $x=-10$ Re (65.7°). However, it is implausible from the current line tracing. The onset region 1 FAC is mapped to the cusp-mantle region through the near earth flow shear between the plasma sheet and the lobe. Correspondence between the plasma sheet and the ionosphere so far believed is quite confusing. It is doubtful to consider that all auroras observed in the ionosphere have their corresponding counterpart in the plasma sheet.

Keywords: substorm

One-month periodicity in thunderstorm, OLR and solar parameters

TAKAHASHI, Yukihiro^{1*} ; SATO, Mitsuteru¹

¹Department of CosmoSciences, Hokkaido University

Recently the relationship between the global circuit and solar-climate connection was pointed out. Here we introduce an example, which indicates the roles of thunderstorm or its resultant electric circuit in solar-climate connection. Global relationship between thunderstorm/cloud activities and solar parameters are examined based on lightning measurement by Global ELF observation Network (GEON) operated by Hokkaido University and Outgoing Longwave Radiation (OLR) intensity. It was found that the number of lightning stokes in Asia Maritime Continent (AMC) varies with about month periodicity in the period from February to June 2004 and shows positive correlation ($R \sim 0.8$) with OLR in the Western Pacific Warm Pool (WPWP). On the other hand, OLRs in the central Africa and some other tropical areas show negative correlation with the number of lightning stokes in the AMC in that period. It is also found that the galactic cosmic rays or UV intensity associated with solar activity indicates good correlation with tropical OLR or lightning activity in AMC. One explanation to connect such global variations in thunderstorm / cloud amount with solar parameters would be the electrical circuit involving lower and upper atmospheres. Global electric circuit model was proposed long time ago, in 1930s, in which thunderstorm plays a role of generator, and the ground and the ionosphere work as a spherical capacitor. However, now we need to reconstruct this simple model, taking into account 3 aspects: 1) global-scale nonuniformities both of ionospheric conductivity and of the distribution of the generators, 2) connections between the troposphere and D-region, considering the effects of TLEs, such sprites and blue jets, 3) establishing the observational methodology for global electric field, excluding the effect of cloud existing just above the observation sites. If the ionospheric electric field modulates the potential gradient in the lower atmosphere, it could cause the re-distribution of ionized atmospheric particles, which may, in turn, change the generation / reduction speed of cloud particles.

Keywords: thunderstorm, OLR, solar activity, one-month periodicity

Influence of solar wind on climate: On the factors such as Quasi Biennial Oscillation

ITOH, Kiminori^{1*} ; MATSUO, Shinya¹ ; YAMASHITA, Kazuyoshi¹

¹Yokohama National University, Graduate School of Env. & Inf. Sciences

In spite of long history of research, the influence of solar changes on the climate is not convincing enough yet. We have employed solar wind parameter (e.g., $P\alpha$ (energy flowing into magnetosphere) and aa index) to successfully show their correlation with the temperatures of the stratosphere, troposphere and surface. For further analyses, OLR (outgoing longwave radiation) and the participation of QBO etc. are studied. For instance, January OLR during 1975-2011 showed high correlation with $P\alpha$ at particular regions. At the QBO westerly phase, high correlation coefficient ($r = 0.76$) was found near Indonesia. The correlation map at the easterly phase resembled that for the Arctic Oscillation, and $r = 0.81$ at the Siberia region.

Keywords: Solar wind, climate, QBO, OLR, temperature

Laboratory experiment with various radiation sources for verification of cloud condensation nucleation by cosmic rays

SUZUKI, Asami^{1*} ; MASUDA, Kimiaki¹ ; TAKEUCHI, Yuya¹ ; ITOW, Yoshitaka¹ ; SAKO, Takashi¹ ; MATSUMI, Yutaka¹ ; NAKAYAMA, Tomoki¹ ; UEDA, Sayako¹ ; MIURA, Kazuhiko² ; KUSANO, Kanya¹

¹Solar-Terrestrial Environment Laboratory, Nagoya University, ²Tokyo university of science

It is considered that the solar activity may affect the global climate, but the correlation mechanism is still not understood.

One of the possible mechanisms for the correlation is the cloud formation by the galactic cosmic rays, which are modulated by the variation of solar activity. This relation was clearly indicated by the good correlation observed for the galactic cosmic-ray intensity and the global low-cloud amount.

This hypothesis includes the ion-induced nucleation model, in which new particles in the atmosphere are created efficiently through atmospheric ions produced by cosmic rays, and finally these particles grow up to the size of cloud condensation nuclei.

In this study, a laboratory experiment for verification of the hypothesis has been conducted with a reaction chamber. A flow of clean air, water vapor, ozone and sulfuric dioxide was introduced to a metallic chamber, where we irradiated UV light for solar irradiance and beta-rays or accelerator beam for cosmic rays. The beam of the heavy ion accelerator HIMAC at National Institute of Radiological Sciences was used in the present experiment.

As a result, ions produced by the ionizing radiation and increased particle density were observed for beta rays.

Some results with the accelerator beam are the following.

Ion density in the chamber increased as the beam intensity and particle density increased with ion density.

Particle size distribution was measured and the peak particle size and the particle density became to larger with time after start irradiation, but the density stopped to increase or decreased after irradiation stopped although the peak size continued to increase.

It is shown that our system is ready for more detailed measurements.

Keywords: cosmic rays, cloud, cosmo-climatology, cloud condensation nuclei

Study on symmetry-breaking between the northern and southern hemispheres of the solar dynamo

SHUKUYA, Daishi^{1*} ; KUSANO, Kanya¹

¹Solar-Terrestrial Environment Laboratory, Nagoya University

Solar dynamo is a mechanism whereby the kinetic energy of the plasma in the sun is converted to the magnetic energy. This mechanism works to generate and maintain all solar magnetic activities. Because the Earth's climate can be influenced by solar activities, variability of the solar dynamo is an important issue to understand long-term evolution of the Earth's climate.

Comparisons of the solar activities in each solar hemisphere show hemispheric asymmetry. Sunspots were found preferentially in one hemisphere and not the other in often long periods of time (Spoerer, 1889; Maunder, 1890, 1904). This asymmetry was extended to other measures of activity including faculae, prominences and flares (Waldmeier, 1971; Roy, 1977). The asymmetry happens in the solar polar magnetic field reversals. The polarity of the solar magnetic fields on the north and south poles periodically reverses at every sunspot maxima. However, the reversals at both poles actually don't occur at the same time. In other words, the reversal at one pole is followed by that on the other pole. This time difference of magnetic field reversals between the poles was first noted by Babcock (1959) from the very first observation of polar field. Recently, it was confirmed by detailed observations with the HINODE satellite (Shiota et al. 2012). As above, we have ever obtained many observation facts. However, the mechanisms of hemispheric asymmetry of the solar dynamo haven't been revealed theoretically yet.

In this paper, we study the asymmetric feature of the solar dynamo based on the flux transport dynamo model (Chatterjee et al. 2004) to explain the time difference of magnetic polarity reversal between the north and south poles. In order to calculate long-term variations of solar activities, we use the mean field kinematic dynamo model, which is derived from magnetohydrodynamics (MHD) equation through the mean field and other approximations. We carried out the mean field dynamo simulations using the updated SURYA code which was developed originally by Choudhuri and his collaborators (2004). We decomposed the symmetric and asymmetric components of magnetic field, which correspond respectively to the quadrupole and dipole-like components (Nishikawa and Kusano 2008), and analyzed the phase relation between them. As a result, we found that the two components are mixed even if the dipole-like component is predominant and that the two components spontaneously form 90 or -90 degree out of phase oscillation. The solutions with 90 and -90 degree out of phase oscillation form the different attractors of dynamo solutions. We found that the time difference of the polar field reversals between the different hemispheres can be explained by the out of phase relation between the different components of magnetic field.

Keywords: polar field reversal, solar dynamo, numerical simulation, hemispheric asymmetry

Climate responses in central Japan and Taiwan to the cosmic ray intensifications during the Maunder Minimum

SAKASHITA, Wataru^{1*}; YOKOYAMA, Yusuke¹; MIYAHARA, Hiroko²; AZE, Takahiro³; YONENOBU, Hitoshi⁴; OHYAMA, Motonari⁵; HOSHINO, Yasuharu⁶; NAKATSUKA, Takeshi⁷

¹Atmosphere and Ocean Research Institute, The University of Tokyo, ²College of Art and Design, Musashino Art University, ³Interactive Research Center of Science, Tokyo Institute of Technology, ⁴Graduate School of Education, Naruto University of Education, ⁵The Center for Academic Resources and Archives, Botanical Gardens, Tohoku University, ⁶National Research Institute for Cultural Properties, Nara, ⁷Research Institute for Humanity and Nature

Relationship between solar variations and climate has been long discussed for various time scales. It is difficult to distinguish the impacts of the multiple solar parameters (total solar irradiance (TSI), solar ultraviolet (UV) radiation, and galactic cosmic rays (GCRs)) on climate, because these variations are nearly synchronized. However, GCR fluctuations related to solar magnetic activity have slightly different features compared to the other external forcing factors (TSI, UV). According to previous studies, the cosmic ray fluctuation was particularly unique during the Maunder Minimum (A. D. 1645-1715), when almost no sunspots were observed. Annually measured tree-ring $\Delta^{14}\text{C}$ and ice-core ^{10}Be data have shown that decadal variations of GCRs had been remarkably amplified during the Maunder Minimum. This characteristic amplification may be utilized to shed light on the GCR influence on climate.

In this study, we employ tree rings that can reconstruct both annual climate ($\delta^{18}\text{O}$) and cosmic ray fluctuations ($\Delta^{14}\text{C}$) during the Maunder Minimum. By using these proxies, we can directly compare these reconstructions without any dating error. Annually measured tree-ring $\delta^{18}\text{O}$ records from central Japan have shown significant wet climate at every remarkable GCRs enhancement. On the other hand, there is no significant climate response in tree-ring $\delta^{18}\text{O}$ record from Taiwan. We suggest that these climate responses may be related to a stationary position of the Baiu front. Recent satellite observations have shown that GCRs may cause the increase of low cloud amount at tropical western Pacific region. It can be suggested that cooling of tropical western Pacific region caused by GCR enhancement might have caused the weakening of Pacific high and indirectly brought wet rainy seasons in central Japan.

Keywords: Solar Magnetic Activity, Galactic Cosmic Ray, The Maunder Minimum, Tree-ring isotope

Dynamical estimation of external/internal acceleration processes of the outer radiation belt using data assimilation

MIYOSHI, Yoshizumi^{1*} ; TOYAMA, Haruto¹ ; UENO, Genta² ; KOSHIISHI, Hideki³ ; MATSUMOTO, Haruhisa³ ; SH-IOKAWA, Kazuo¹

¹STEL, Nagoya University, ²The Institute of Statistical Mathematics, ³JAXA

Dynamical evolution of the outer belts should be a delicate balance among several processes. It has been believed that there exist two different acceleration mechanisms: the radial diffusion as the external source process, and the non-adiabatic wave particle interactions as the internal source process. In order to discriminate when and where these processes are dominant for the large flux enhancement of the outer belt electrons, we have developed a data assimilation code on the outer belt electrons. In our data assimilation, the particle filter and the particle smoother are used which are effective for non-linear/non-Gaussian distribution problems. We include the radial diffusion coefficient and the internal source model in the state vector and estimate the dynamical variations of these parameters. The Tsubasa satellite electron data are used as the observation vector. The results indicate that only the radial diffusion process is always too small to explain the observed flux enhancement and the internal source process should be necessary. The assimilation result suggests that the internal source process tend to take place around the storm recovery phase, which is consistent with the observations.

Keywords: radiation belts, data assimilation

Evaluation of Relativistic Electron Flux Forecast at GEO Satellite

NAGATSUMA, Tsutomu^{1*} ; SAKAGUCHI, Kaori¹ ; SAITO, Shinji² ; MIYOSHI, Yoshizumi² ; SEKI, Kanako²

¹National Institute of Information and Communications Technology, ²Solar Terrestrial Environment Laboratory, Nagoya University

We have developed near real time prediction model for relativistic electron flux at GEO satellite. This model is based on a multivariate autoregressive model with using solar wind speed, north-south component of the magnetic field and dynamic pressure as inputs. Detailed description of this model can be found in Sakaguchi et al. [2013]. We have started relativistic electron flux forecast service as a test product since Apr. 2013. Forecast information can be found in the following web pages (URL: <http://seg-web.nict.go.jp/radi/>).

There are several difficulties in operating a near-real time forecast model. One is the quality of the real-time solar wind data. Because quality of real-time solar wind density data is quite poor, we avoid using solar wind density data for our operational model. The other one is the lead-time of the solar wind data. Currently, we can use only ACE data for solar wind input. The lead-time of this data is only about one hour. Therefore, we also 'predict' solar wind condition for two or three days in advance from current solar wind information. Anyway, prediction efficiencies of our forecast for 1day, 2day, and 3day ahead in 2013 are 81%, 63%, 48%, respectively. Evaluation and future perspective of our forecasting model will be introduced in our presentation.

Reference:

Sakaguchi, K., Y. Miyoshi, S. Saito, T. Nagatsuma, K. Seki and K. T. Murata (2013), Relativistic electron flux forecast at geostationary orbit using Kalman filter based on multivariate autoregressive model, *Space Weather*, 11, 79-89, doi:10.1002/swe.20020.

Keywords: Space Weather Forecast, Solar Wind - Magnetosphere Interaction, Magnetosphere, Radiation Belt, Inner Magnetosphere, Modeling

Maps of ionospheric conductances, currents, and convection from the Swarm multi-satellite mission

AMM, Olaf^{1*} ; VANHAMAKI, Heikki¹ ; KAURISTIE, Kirsti¹ ; STOLLE, Claudia⁴ ; CHRISTIANSEN, Freddy³ ; HAAGMANS, Roger⁵ ; MASSON, Arnaud⁶ ; TAYLOR, Matt⁵ ; FLOBERGHAGEN, Rune⁷ ; ESCOUBET, Philippe⁵

¹Finnish Meteorological Institute, Arctic Research Unit, Helsinki, Finland., ²STEL, Nagoya University, Japan, ³Technical University of Denmark, DTU Space, Lyngby, Denmark, ⁴Helmholtz-Centre Potsdam, GFZ German Research Center for Geosciences, Germany, ⁵ESTEC, Noordwijk, The Netherlands, ⁶ESAC, Madrid, Spain, ⁷Directorate of Earth Observation Programmes, ESRIN, Frascati, Italy

The recently launched ESA Swarm spacecraft mission is the first dedicated multi-satellite ionospheric mission with two low-orbiting spacecraft that are flying in parallel in a distance of ~ 100 km, thus allowing to derive spatial gradients of ionospheric parameters not only along the orbits, but also in the direction perpendicular to them. In addition, a third satellite with a slightly higher orbit regularly crosses the paths of the lower spacecraft pair. Using the Swarm magnetic and electric field instruments, we present a novel technique that allows to derive 2-dimensional (2D) maps of ionospheric conductances, currents, and convection in the area between the trajectories of the two parallel flying spacecraft, and even to some extent outside of it. This technique is based on Spherical Elementary Current Systems (SECS). We present several test cases of modelled ionospheric situations from which we calculate virtual Swarm data, and show that the technique is able to reconstruct the model electric field (or convection), horizontal currents, and conductances with very good to excellent accuracy. Larger errors arise for the reconstruction of the 2D field-aligned currents (FAC) map, especially in the area outside of the spacecraft orbits. However, even in this case the general pattern of the model FAC is recovered, and the magnitudes are valid in an integrated sense. Finally, using an MHD model run, we show how our technique allows to estimate the ionosphere-magnetosphere coupling parameter K , if conjugate multi-point observations of the magnetospheric magnetic and electric field are available, as they can be obtained, e.g., from the ESA Cluster mission.

Keywords: ionosphere, ionospheric electrodynamics, ionospheric currents, ionospheric convection, magnetosphere-ionosphere coupling, Swarm mission

MLT and seasonal dependence of auroral electrojets: IMAGE magnetometer network observations

GUO, Jianpeng^{1*} ; LIU, Huixin²

¹SIGMA Weather Group, State Key Laboratory of Space Weather, CSSAR, Chinese Academy of Sciences, ²Department of Earth and Planetary Sciences, Faculty of Sciences, Kyushu University

Total eastward and westward electrojet currents (EEJ and WEJ) and their central latitudes derived from the IMAGE network magnetic measurements are analyzed for the combined MLT and seasonal dependence during the period 1995-2009. EEJ shows a strong MLT variation with significant dependence on season. During summer months the maxima occur around 1600-1800 MLT, whereas during winter months the maxima occur at a later local time sector around 1800-2000 MLT. Moreover, the summer maxima are much larger than the winter maxima, and appear at higher latitudes. The summer maxima are mainly associated with the solar EUV conductivity effect, while the winter maxima are mainly due to the contribution of northward convective electric field. EEJ exhibits a dominant annual variation with maximum in summer and minimum in winter. WEJ also exhibits a strong MLT variation with significant dependence on season. The maxima occur around 0200-0400 MLT during summer months, around 0000-0200 MLT during winter months, and around 0000-0400 MLT during equinoctial months. Moreover, the equinoctial maxima are much larger than the summer and winter maxima, and appear at relatively lower latitudes. The seasonal variations in WEJ are the combinations of annual variations and semiannual variations. Both annual and semiannual variations show significant dependence on MLT. These results increase our knowledge on what factors contribute to the auroral electrojets as well as their magnetic signatures, and hence help us better understand the limitations of global auroral electrojet indices, such as the AE and SME indices.

Temporal variations of nitric oxide in the mesosphere and lower thermosphere over Syowa station, Antarctica

ISONO, Yasuko¹ ; MIZUNO, Akira^{1*} ; NAGAHAMA, Tomoo¹ ; MIYOSHI, Yoshizumi¹ ; NAKAMURA, Takuji² ; KATAOKA, Ryuhō² ; TSUTSUMI, Masaki² ; EJIRI, Mitsumu² ; FUJIWARA, Hitoshi³ ; MAEZAWA, Hiroyuki⁴ ; UEMURA, Miku¹

¹Solar-Terrestrial Environment Laboratory, Nagoya University, ²National Institute of Polar Research, ³Seikei University, ⁴Osaka Prefecture University

Energetic particle precipitation (EPP) related to solar proton events or geomagnetic storms induce ion-neutral reactions and change abundance of some minor molecules such as NO_x and HO_x in the mesosphere and lower thermosphere. To investigate the temporal variations of NO by EPP, we installed a millimeter-wave spectroscopic radiometer at Syowa Station (69.00S, 39.85E), and we have carried out ground-based observations of spectral line of nitric oxide (NO) at 250.796 GHz since January 2012.

We obtained 197 and 172 daily averaged NO spectra in 2012 and 2013 (until 30 September; DOY 273), respectively. The daily NO spectra are characterized by narrow line width with a Full-Width-at-Half-Maximum (FWHM) of about 0.5 MHz. These NO spectra are well fitted by a single Gauss function or by a single Lorenz function. From the spectral line shape, we conclude that the NO emitting region is between 75 and 100 km.

We found two temporal variation patterns of NO column density. One is a seasonal variation with a maximum in the winter and a minimum in the summer. The column density of NO during the winter was about 4 times larger than that during the summer. This seasonal variation is considered to be related to the atmospheric transport and the NO dissociation by solar radiation. The other is the short-term variation in a timeframe of 5-10 days associated with EPP events such as solar proton events and geomagnetic storms. At Syowa Station, short-term variations were caused mainly by the precipitation of electrons rather than that of protons. In the electron precipitation events, the column density of NO gradually increases just after the main phase of the geomagnetic storm and gradually decreases soon after its peak.

One of the short-term events related to a large geomagnetic storm in April 2012 was the most prominent single event among those observed at Syowa Station since January 2012. From the high time resolution (~ 3-hour) data, we revealed a diurnal tendency that NO column density increased about twice at UT 0, which is interpreted to be caused by the dawn-dusk asymmetry of the precipitated electrons with energies 30-300 keV.

Keywords: Nitric oxide, mesosphere and lower thermosphere, energetic particle precipitation, geomagnetic storm, solar proton event, Antarctica

The Impacts of Space Weather on Society and the Economy

BAKER, Daniel N.^{1*}

¹University of Colorado Boulder

This presentation describes possible extreme space weather impacts and their economic and societal costs. Modern society depends heavily on a variety of technologies that are vulnerable to the effects of intense geomagnetic storms and solar energetic particle (SEP) events. Strong currents flowing in the ionosphere can disrupt and damage Earth-based electric power grids and contribute to the accelerated corrosion of oil and gas pipelines. Magnetic storm-driven ionospheric disturbances interfere with high-frequency radio communications and navigation signals from Global Positioning System (GPS) satellites. Exposure of spacecraft to solar particles and radiation belt enhancements can cause temporary operational anomalies, damage critical electronics, degrade solar arrays, and blind optical systems such as imagers and star trackers. Moreover, intense SEP events present a significant radiation hazard for astronauts during the high-latitude segment of the International Space Station (ISS) orbit as well as for future human explorers of the Moon and Mars. In addition to such direct effects as spacecraft anomalies or power grid outages, a thorough assessment of the impact of severe space weather events on present-day society must include the collateral effects of space-weather-driven technology failures. For example, polar cap absorption events due to solar particles can degrade — and, during severe events, completely black out — radio communications along transpolar aviation routes, requiring aircraft flying these routes to be diverted to lower latitudes. This can add considerable cost to the airlines and can greatly inconvenience passengers. Modern technological society is characterized by a complex set of interdependencies among its critical infrastructures. A complete picture of the socioeconomic impact of severe space weather must include both direct as well as collateral effects of space-weather-driven technology failures on dependent infrastructures and services.

Keywords: Space weather, Electric power grids, Radiation hazards, Infrastructure interdependencies, Socioeconomic impact of severe space weather

GEMSIS-Sun Numerical Model of Sun-Earth System (SUSANOO): Application for Extremely Strong IMF CMEs

SHIOTA, Daikou^{1*} ; KATAOKA, Ryuh² ; MIYOSHI, Yoshizumi¹ ; KUSANO, Kanya¹

¹STEL, Nagoya University, ²National Institute of Polar Research

Solar wind including coronal mass ejections (CMEs) is a main driver of various space weather disturbances. MHD modeling of the solar wind is a powerful tool to understand the solar-terrestrial environment and to forecast space weather accurately. Recently, we developed an MHD model of the inner heliosphere on the basis of minimal input, namely, time series of daily synoptic observation of the photospheric magnetic field. The time series of MHD parameters at the Earth position is passed to a radiation belt model [Miyoshi et al. 2004] for forecasting of the radiation belt energetic electron flux. These programs are executed everyday on a server in STEL, Nagoya University and the results are uploaded on the web site (<http://st4a.stelab.nagoya-u.ac.jp/susanoo/>). This system is named as Space-weather-forecast-Usable System Anchored by Numerical Operations and Observations (SUSANOO).

Carrington event that occurred in September 1859 is the most violent solar storm in the human records. Since the magnetic storm associated with the event influenced globally, aurora was observed in wide area in the world. The magnetic response recorded in Bombay shows a rapid decrease of -1600 nT/h (Tsurutani et al. 2003). The induced electric field to explain the rapid decrease in the ground level is estimated to be 355 mV/m associated with a magnetic cloud influence. The time lag between onsets of solar flare and sudden commencement is 17.5 hours, and therefore shock propagation speed is estimated as 2380 km/s . The magnetic field strength in the associated magnetic cloud is needed to be 150 nT . However, it is not clear how such a strong magnetic field can be kept while the strength of ordinary interplanetary magnetic field (IMF) is the order of 10 nT at 1 au .

In order to examine which condition of coronal mass ejections (CMEs) associated with an extreme event such as the Carrington event should be satisfied, we modeled a series of CMEs with the inner heliosphere MHD simulation (used in SUSANOO). In the model, multiple CMEs are injected as a twisted magnetic flux rope accompanying with a velocity pulse through the inner boundary of the simulation and propagate into the solar winds. Because there is almost no information associated with the Carrington event and the solar wind, instead, we used observational data of CMEs associated recent large-scale active regions: NOAA 10486 in October to November 2003 (Halloween event) and NOAA 11520 in July 2012 (far side STEREO event, Russell et al. 2013). Only fast ($V > \sim 1000 \text{ km/s}$) and wide (angular width > 60 degree) CME data are extracted from LASCO CME catalog (http://cdaw.gsfc.nasa.gov/CME_list/). As a result, the strength of compressed magnetic field becomes as high as about four times of background IMF when a CME interacts with the background solar wind. However, successive CMEs interact with each other to form much stronger magnetic field due to compression of the magnetic cloud of the preceding CME by shock associated the following CME.

Keywords: MHD, coronal mass ejection, solar wind, IMF, geomagnetic storm, radiation belt

Discovery of Two Sun-like Superflare Stars Rotating as Slow as the Sun

NOGAMI, Daisaku^{1*}; NOTSU, Yuta¹; HONDA, Satoshi²; MAEHARA, Hiroyuki³; NOTSU, Shota¹; SHIBAYAMA, Takuya¹; SHIBATA, Kazunari¹

¹Kyoto University, ²University of Hyogo, ³The University of Tokyo

We report on the results of high dispersion spectroscopy of two ‘superflare stars’, KIC 9766237, and KIC 9944137 with Subaru/HDS. Superflare stars are G-type main sequence stars, but show gigantic flares compared to the Sun, which have been recently discovered in the data obtained with the Kepler spacecraft. Though most of these stars are thought to have a rotation period shorter than 10 days on the basis of photometric variabilities, the two targets of the present paper are estimated to have a rotation period of 21.8 d, and 25.3 d. Our spectroscopic results clarified that these stars have stellar parameters similar to those of the Sun in terms of the effective temperature, surface gravity, and metallicity. The projected rotational velocities derived by us are consistent with the photometric rotation period, indicating a fairly high inclination angle. The average strength of the magnetic field on the surface of these stars are estimated to be 1-20 G, by using the absorption line of Ca II 8542. We could not detect any hint of binary in our spectra, although more data are needed to firmly rule out the presence of an unseen low-mass companion. These results claim that the spectroscopic properties of these superflare stars are very close to those of the Sun, and support the hypothesis that the Sun might cause a superflare.

Keywords: Sun-like stars, superflares, high dispersion spectroscopy